ORIGINAL ARTICLE

Application of a medium-energy collimator for I-131 imaging after ablation treatment of differentiated thyroid cancer

Masato Kobayashi · Hiroshi Wakabayashi · Daiki Kayano · Takahiro Konishi · Hironori Kojima · Hiroto Yoneyama · Koichi Okuda · Hiroyuki Tsushima · Masahisa Onoguchi · Keiichi Kawai · Seigo Kinuya

Abstract

Purpose High-energy (HE) collimators are usually applied for I-131 imaging after ablation treatment of differentiated thyroid cancer (DTC). However, purchase of HE collimators has been avoided in many nuclear medicine departments because the HE collimators are more expensive than other collimators. In this study, we compared the I-131 imaging using HE- and medium-energy (ME) collimators, which is more versatile than HE collimators.

Materials and methods To simulate DTC patients with extra-thyroid beds, a phantom of acrylic containers containing I-131 was used. To simulate patients with thyroid beds, four phantoms representing extra-thyroid beds were arranged around the phantom representing normal thyroid tissues. Patients administered 1.11 or 3.70 GBq NaI-131 were also evaluated. Whole-body imaging and SPECT imaging of the phantoms and patients performed using HE-general-purpose (HEGP) and ME-low-penetration (MELP)

collimators, and full-width at half maximum (FWHM) and percent coefficient of variation (%CV) were measured.

Results In the extra-thyroid beds, FWHM and %CV with MELP were negligibly different from those with HEGP in whole-body imaging. Although FWHM with MELP was a little different from that with HEGP in SPECT imaging, %CV with MELP was significantly higher than that with HEGP. In the thyroid beds, only an extra-thyroid bed including higher radioactivity was identified in whole-body imaging with both collimators. Although SPECT images with MELP could not clarify extra-thyroid beds with low radioactivity, HEGP could identify them. In patients, although some whole-body images with MELP could not detect extra-thyroid beds, whole-body imaging with HEGP and SPECT imaging with both collimators could detect them.

Conclusions Although HEGP is the best collimator for I-131 imaging, MELP is applicable for not only whole-body imaging but also SPECT imaging.

Keywords NaI-131 · Ablation · Differentiated thyroid cancer · Medium-energy collimator · High-energy collimator

M. Kobayashi (✉) · M. Onoguchi · K. Kawai
School of Health Sciences, College of Medical, Pharmaceutical and Health Sciences, Kanazawa University, 5-11-80 Kodatsuno, Kanazawa 920-0942, Japan
e-mail: kobayasi@mhs.mp.kanazawa-u.ac.jp

H. Wakabayashi · D. Kayano · K. Okuda · S. Kinuya
Department of Biotracer Medicine, Kanazawa University Graduate School of Medical Sciences, Kanazawa, Japan

T. Konishi · H. Kojima · H. Yoneyama
Department of Radiology, Kanazawa University Hospital, Kanazawa, Japan

H. Tsushima
Department of Radiological Sciences, Ibaraki Prefectural University of Health Sciences, Ibaraki, Japan

Introduction

A capsule including radioactive sodium iodine-131 (NaI-131) is administered orally for ablation treatment of differentiated thyroid cancer (DTC) [1–3]. Ablation treatment with I-131 >1.11 GBq (30 mCi) is often performed on an inpatient basis, whereas treatment with I-131 ≤1.11 GBq is often done on an outpatient basis [4, 5].

I-131 imaging with whole-body and SPECT scanning is a useful tool for identifying the location of DTC or

metastases and evaluating the effect of the treatment [6–8]. Selection of the appropriate collimator is important to obtain clear images in nuclear medicine imaging. In general, high-energy (HE) and medium-energy (ME) collimators are used for energy range of 300–500 and 150–300 keV, respectively. Although HE collimators are ideally applied for I-131 imaging because of the high photon energy of I-131 [9, 10], the HE collimators are more expensive than that of other collimators and the purchase of HE collimators has been avoided for many nuclear medicine departments in hospital. In this case, medium-energy (ME) collimators have been used for I-131 imaging [11, 12]. However, the suitability of ME collimators for I-131 imaging has not been extensively evaluated. In this study, we compared I-131 imaging after ablation treatment of DTC using ME and HE collimators. The image quality was evaluated using phantoms to simulate a single extra-thyroid bed and thyroid beds containing cancer, as in patients with DTC. The I-131 radioactivity was estimated as 1.11 GBq for outpatients and 3.70 GBq (100 mCi) for inpatients.

Materials and methods

Point source and phantoms

Performance tests with ME-low-penetration (MELP) and HE-general-purpose (HEGP) collimators were performed to measure the system resolution and sensitivity in planar imaging at 10 cm from a 37 MBq (1 mCi) I-131 point source.

Image and size of phantom and schematic layout for simulation of thyroid beds are also shown in Fig. 1. An acrylic cylindrical container (20 mm in diameter and 10 mm thick, with a 5-mm diameter cylindrical hole) was used as a phantom to simulate uptake of extra-thyroid beds and thyroid beds after thyroidectomy (Fig. 1a, b). To simulate the extra-thyroid beds including lymph node metastases, the phantoms containing 1.85 MBq (50 μCi) I-131 were placed in the center of the field of view (FOV) in the images.

To simulate thyroid beds, four phantoms containing 5.55 or 18.5 MBq (0.15 or 0.5 mCi) were placed in the center of the FOV, and four phantoms including 0.19, 0.37, 0.74 or 1.85 MBq (5, 10, 20 or 50 μCi) were set up around the four phantoms representing normal thyroid tissues to simulate extra-thyroid beds (Fig. 1c). These containers were placed on an acrylic board, which simulated the body of a patient. The acrylic board was placed on the table for patients in the SPECT scanner (Fig. 1d). The I-131 radioactivity was determined by measuring the radiation exposure of patients using the medical internal radiation dose (MIRD) method
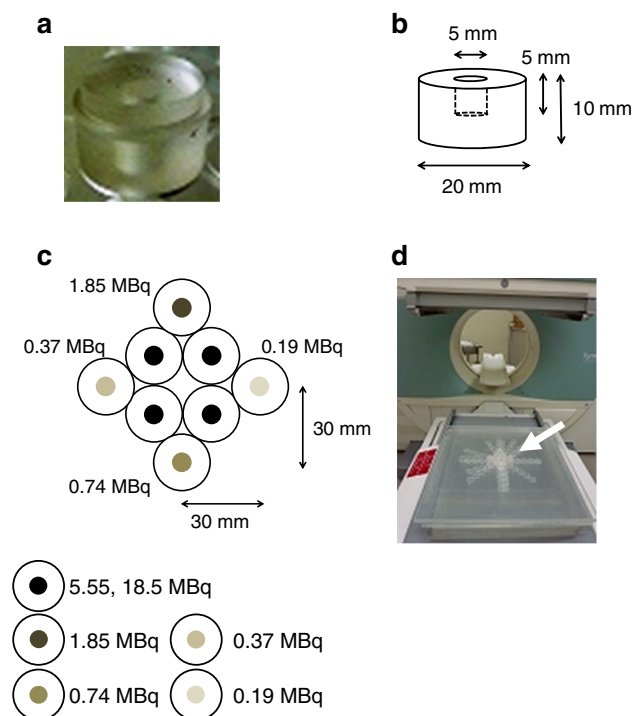
Fig. 1 Image and size of phantom and schematic layout were shown as simulation of thyroid beds. Image of phantom simulating single extra-thyroid beds and thyroid beds (**a**); size of phantom (**b**); schematic layout of thyroid beds (**c**); and phantom set-up (*solid arrow*) on patient bed (**d**). In the thyroid beds, four phantoms containing 5.55 or 18.5 MBq of I-131 simulated normal thyroid tissues and four phantoms including 0.19, 0.37, 0.74 or 1.85 MBq of I-131 were placed around these phantoms to simulate extra-thyroid beds

at 3 days after oral administration of 1.11 or 3.70 GBq NaI-131 for ablation.

SPECT/CT camera

The SPECT scanner was equipped with a dual-head gamma camera with 9.5-mm-thick NaI crystals, had a 38.7 × 53.3 cm FOV, and was combined with a spiral 6-slice CT (80, 110 and 130 kV, 20–345 mA, and 0.8, 1.0 and 1.5 s rotation time) in the same gantry (SymbiaT6; Siemens Medical Solutions, Erlangen, Germany) [14]. HEGP and MELP collimators were selected for the I-131 imaging study. The specifications of the HEGP and MELP collimators are presented in Table 1.

Whole-body and SPECT image acquisition in phantoms

Whole-body and SPECT acquisition methods with NaI-131 for the ablation were established in our previous study [13]. For whole-body imaging, each collimator was 10 cm from the phantom. Images were acquired at table speeds of 10, 15 or 20 cm/min using a 256 × 1024 matrix (2.4-mm pixel

Table 1 Collimator specifications of MELP and HEGP

Collimator Isotope	MELP Ga-67	HEGP I-131
Hole shape	Hexagonal	Hexagonal
Number of holes (×1000)	14	8
Hole length (mm)	40.64	50.80
Septal thickness (mm)	1.14	2.00
Hole diameter (mm across the flats)	2.94	3.40
Sensitivity at 10 cm (cpm/kBq)	8.38	3.84
System resolution at 10 cm (mm)	12.5	14.6
Septal penetration (%)	1.2	3.5

size) and a 364-keV photopeak with a 15 % window. SPECT images were scanned using step and shoot with 60 projections (6 degrees/projection) for 360-degree acquisition at 20 s per projection. Image matrix sizes and the scan energy window were a 256×256 matrix and zoom 1 (2.4-mm pixel size), a 128×128 matrix and zoom 1 (4.8-mm pixel size) and a 364-keV photopeak with a 15 % window. After SPECT scans, CT transmission scans were performed at 130 kV with a rotation time of 0.6 s. The slice thickness of CT images was set at 4.8 mm (default image slice).

Whole-body and SPECT scans in patients

Two female patients, 46 and 54 years old, with thyroglobulin (Tg) level (<5 and 482 ng/mL, respectively) were administered 1.11 GBq I-131, and two male patients, 58 and 73 years old, with Tg level (282 and 157 ng/mL, respectively) were administered 3.70 GBq I-131. Whole-body and SPECT images of NaI-131 at a therapeutic radioactive dose of 1.11 or 3.70 GBq were acquired at 3 days after NaI-131 administration. The study was approved by the ethics committee of our hospital. Written informed consent was obtained from each subject. From the results of a previous study [13], whole-body scans were performed using a table speed of 15 cm/min, and SPECT scans were obtained using step-and-shoot with 60 projections (6 degrees/projection) for 360-degree acquisition at 20 s per projection. The image matrix size and scan energy window were a 128×128 matrix and zoom 1 (4.8-mm pixel size) and a 364 keV photopeak with a 15 % window and 15 % sub-window for scatter correction with triple energy window. Attenuation correction was performed using CT. In patients, SPECT and CT images were obtained covering areas of the cervical region/thyroid bed and suspected abnormal accumulation on whole-body images.

Reconstruction of SPECT data

SPECT data were reconstructed using ordered subsets expectation maximization (OSEM) with a three-

Table 2 FWHM and %CV of the whole-body imaging with I-131 of 1.85 MBq

Table speed (cm/min)	FWHM (mm)		%CV	
	MELP	HEGP	MELP	HEGP
10	15.9	15.5	28.2	27.6
15	16.1	15.8	30.0	29.6
20	16.2	16.2	39.4*	38.6

* $P < 0.05$ vs. HEGP

dimensional (3D) (OSEM-3D) algorithm, called Flash $3D^{TM}$ in Siemens Medical Solutions [15]. The OSEM-3D algorithm included depth-dependent detector response modeling resolution recovery, attenuation correction, scatter correction and a Gaussian post-filter with twofold full-width at half maximum (FWHM) of pixel size. In the OSEM-3D algorithm, subset and iteration were, respectively, set up to 12 and 10 because the combination of subset and iteration improved recovery coefficients compared with other combinations [15]. In addition, scatter correction was not applied to the phantom study because there was no background activity.

Imaging and statistical analysis

An approximately 5-mm region of interest (ROI) was located in the center of the phantom. The ROI was the same size as the hole in the phantoms. The resolution was measured by FWHM (mm), and image noise was defined as the coefficient of variation (%CV, standard deviation/mean $\times$ 100 (%)) of pixel values within an ROI. Image J was applied to obtain profile curves on SPECT images with both collimators [16]. A statistical software package (JMP® version 9 SAS Institute Inc., Cary, NC, USA) was used for statistical analysis using a paired t test. Statistically significant differences were defined as $P < 0.01$ or 0.05.

Results

System resolution and sensitivity using MELP were, respectively, 14.8 mm and 9.82 cpm/kBq at 10 cm from the I-131 point source, whereas HEGP showed 14.6 mm and 3.84 cpm/kBq.

For the simulation of the extra-thyroid beds, FWHM and %CV on whole-body images using 1.85 MBq I-131 are shown in Table 2. Although FWHM and %CV with MELP were negligibly different from those with HEGP at all table scan speeds, the %CV showed a significantly high value at a table speed of 20 cm/min ($P < 0.05$). Table 3 shows FWHM on the SPECT imaging with different pixel

Table 3 FWHM of the SPECT imaging with different pixel sizes and I-131 radioactivity

FWHM (mm)								
Radioactivity (MBq)	0.19		0.37		0.74		1.85	
Pixel size (mm)	MELP	HEGP	MELP	HEGP	MELP	HEGP	MELP	HEGP
2.4	11.5	11.3	11.3	10.9	11.0	10.8	10.9	10.6
4.8	12.6	12.4	12.6	12.2	12.6	12.1	12.3	12.2
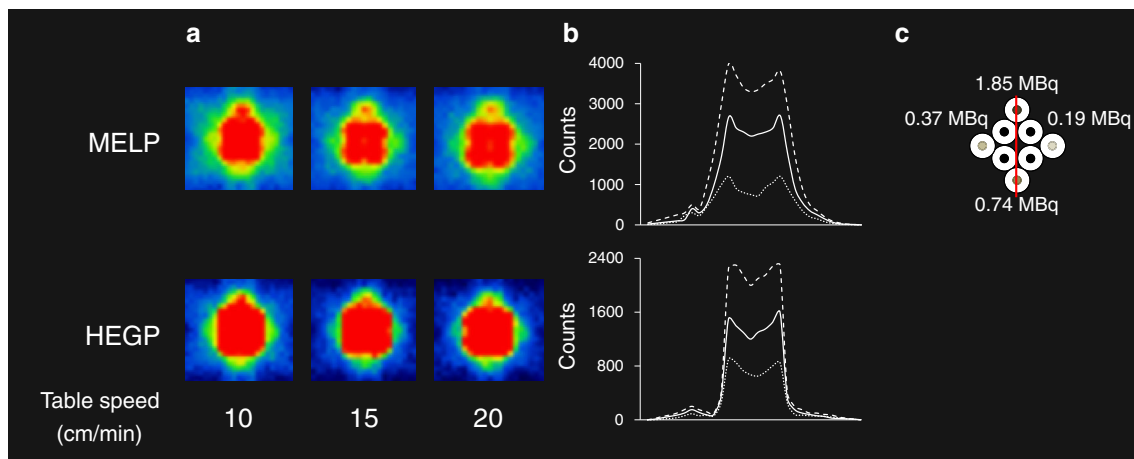
Fig. 2 Whole-body images (**a**), profile curves (**b**) and schematic layout (**c**) were showed using simulated thyroid beds estimating patients administered 1.11 GBq of I-131. On schematic layout, *vertical line* was located to obtain profile curves. In profile curves and the images with both collimators, although only the extra-thyroid beds including 1.85 MBq were distinguished from phantoms simulating normal thyroid tissues at all table speeds of 10 (*dashed line*), 15 (*solid line*) and 20 cm/min (*dotted line*), other extra-thyroid beds were not confirmed because MELP yielded more radioactive scatter than HEGP

sizes and I-131 radioactivity. There were no significant differences in FWHM between MELP and HEGP at pixel sizes of 2.4 and 4.8 mm. However, %CV of MELP was significantly higher than that of HEGP ($P < 0.01$).

In the simulation of the thyroid beds of DTC patients administered 1.11 GBq I-131, only the 1.85 MBq phantom simulating an extra-thyroid bed was differentiated from phantoms simulating normal thyroid tissues on the whole-body imaging using both MELP and HEGP (Fig. 2). On the other hand, SPECT images with HEGP identified the 0.19 MBq phantom, whereas MELP could not identify the 0.19 and 0.37 MBq phantoms (Fig. 3). These results showed the same tendency with the simulation of the thyroid beds for estimating patients administered 3.70 GBq I-131 (data not shown).

Whole-body and SPECT images of two patients administered 1.11 GBq are shown in Figs. 4 and 5. In a patient with low uptake of I-131 in the thyroid beds (Fig. 4), I-131 thyroid uptake with MELP in the whole-body imaging (Fig. 4a) was much lower than that with HEGP and SPECT imaging with both collimators (Fig. 4b–d). In whole-body images of another patient with high uptake of I-131 in the thyroid beds, extra-thyroid beds could not be detected using MELP (Fig. 5a), but could be detected using HEGP (Fig. 5c). On the other hand, SPECT images could differentiate extra-thyroid beds and thyroid beds using both collimators (Fig. 5b, d).

Whole-body and SPECT images of two patients administered 3.70 GBq are shown in Figs. 6 and 7. In a patient with lower uptake of I-131 in the thyroid beds, although whole-body images with MELP could not detect the thyroid beds, whole-body imaging with HEGP and SPECT imaging with both collimators could detect the thyroid beds (Fig. 6). In whole-body images of another patient with high uptake of I-131 into the thyroid beds, whole-body and SPECT images using both collimators could differentiate the thyroid beds (Fig. 7).

Discussion

I-131 imaging is necessary to confirm the efficacy of ablation treatment because treatment and care for patients with thyroid beds and/or lymph node metastases differ from those for patients without thyroid beds and/or lymph node metastases [10, 17]. Although selecting the
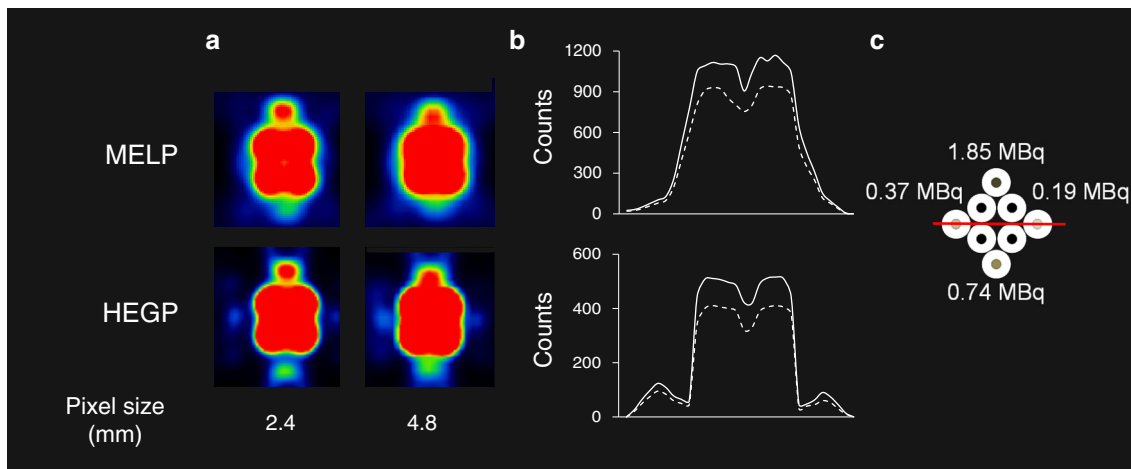
Fig. 3 SPECT images (**a**), profile curves (**b**) and schematic layout (**c**) were shown using simulated thyroid beds estimating patients administered 1.11 GBq of I-131. On schematic layout, *horizontal line* was located to obtain profile curves. In the profile curves, *dashed line* showed the results of SPECT scan with 2.4-mm pixel size and *solid line* showed those of SPECT scan with 4.8-mm pixel size. In the SPECT images with HEGP were able to differentiate the thyroid beds including 0.19 and 0.37 MBq from phantoms simulating normal thyroid tissues compared to those with MELP, although the effect of pixel size was small
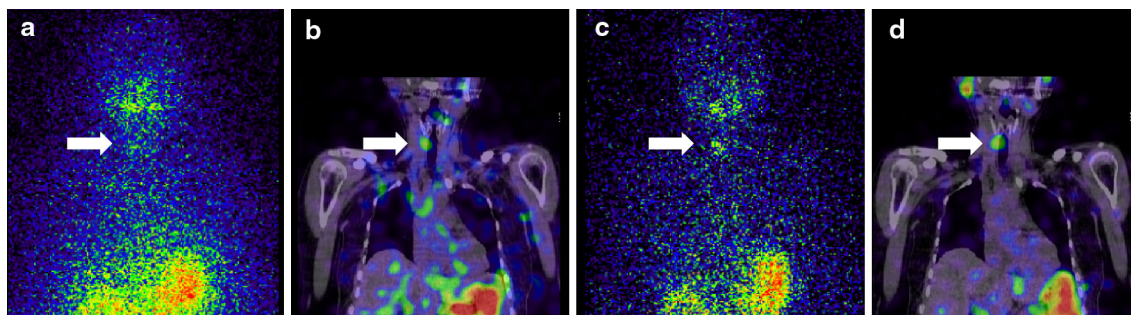
Fig. 4 Thyroid beds in a 46-year-old female patient after ablation treatment with 1.11 GBq I-131. There was lower uptake of I-131 in thyroid beds in patients administered 1.10 GBq. **a** A whole-body image with MELP showed low uptake in the thyroid beds (*solid arrow*). On the other hand, **b** a SPECT image with MELP, **c** a whole-body image with HEGP, and **d** a SPECT image with HEGP showed higher uptake in the thyroid beds compared to a whole-body image with MELP (*solid arrow*). The serum stimulated thyroglobulin level at I-131 ablation was <5 ng/mL. Although whole-body images with MELP could not detect the thyroid beds, whole-body imaging with HEGP and SPECT imaging with both collimators could detect the thyroid beds
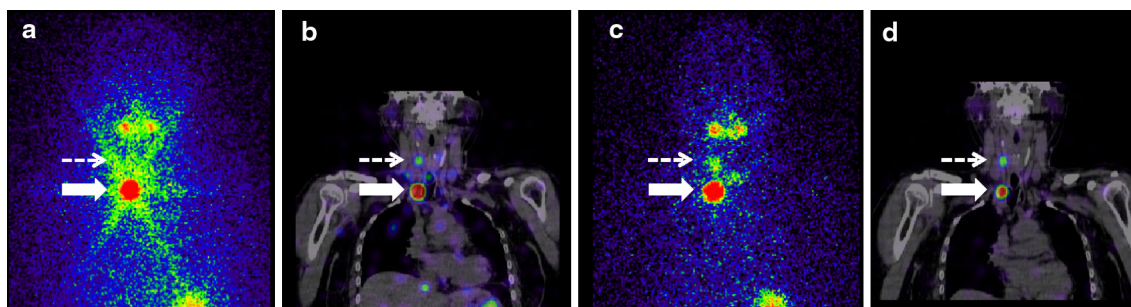
Fig. 5 A 54-year-old female patient with extra-thyroid beds after ablation treatment with 1.11 GBq I-131. There was higher uptake of I-131 in thyroid beds in patients administered 1.10 GBq. **a** A whole-body image with MELP caused many star artifacts (*solid arrow*). On the other hand, **b** a SPECT image with MELP, **c** a whole-body image with HEGP, and **d** a SPECT image with HEGP identified thyroid beds (*solid arrow*) and extra-thyroid beds (*broken arrow*). The serum stimulated thyroglobulin level at I-131 ablation was 482 ng/mL. Extra-thyroid beds could not be detected using MELP, but could be detected using HEGP. SPECT images could differentiate extra-thyroid beds and thyroid beds using both collimators
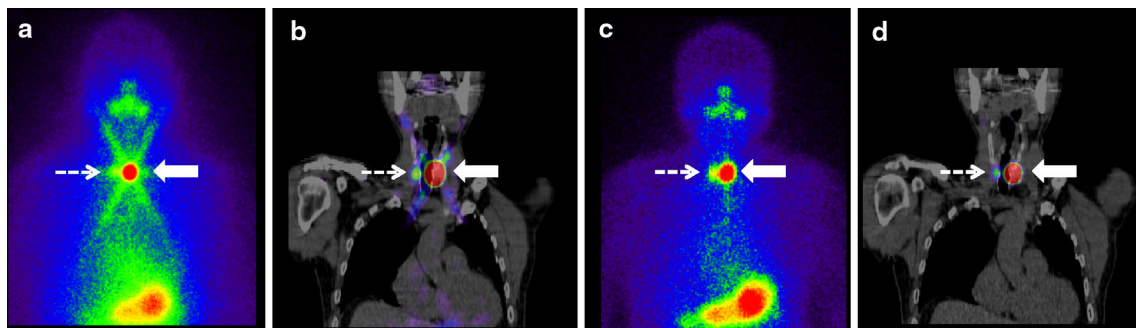
Fig. 6 Thyroid beds in a 58-year-old male patient after ablation treatment with 3.70 GBq I-131. There was lower uptake of I-131 in the thyroid beds in patients administered 3.70 GBq. **a** A whole-body image with MELP showed a large star artifact (*solid arrow*). **b** A SPECT image with MELP, **c** a whole-body image with HEGP, and **d** a SPECT image with HEGP identified thyroid beds (*solid arrow*) and extra-thyroid beds (*broken arrow*). The serum stimulated thyroglobulin level at I-131 ablation was 282 ng/mL. Although whole-body images with MELP could not detect the thyroid beds, whole-body imaging with HEGP and SPECT imaging with both collimators could detect the thyroid beds
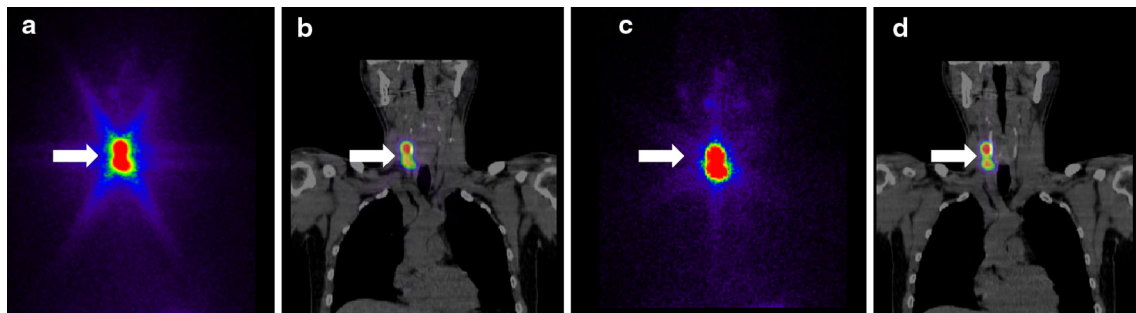
Fig. 7 A 73-year-old male patient with extra-thyroid beds after ablation treatment with 3.70 GBq I-131. There was higher uptake of I-131 in thyroid beds in patients administered 3.70 GBq. **a** A whole-body image with MELP, **b** a SPECT image with MELP, **c** a whole-body image with HEGP, and **d** a SPECT image with HEGP differentiated the thyroid beds (*solid arrow*). The serum stimulated thyroglobulin level at I-131 ablation was 157 ng/mL. In this case, whole-body and SPECT images using both collimators could differentiate the thyroid beds

appropriate collimator is important to obtain clear I-131 images, the costs of the collimators are important for many hospitals. Especially, HE collimators are not economical because they can only be applied for I-131 (mainly 364 keV) imaging. ME collimators are usually applicable for gallium-67 (mainly 93 and 184 keV), indium-111 (171 and 245 keV), indine-123 (mainly 159 keV) imaging, etc. Although the yields of ME collimators can be estimated, ME collimators have more star artifacts than HE collimators because ME collimators are thinner and have more septal penetration. ME collimators are, however, more versatile than HE collimators. In this study, MELP was applied for I-131 imaging after ablation treatment of DTC. The system resolution and sensitivity of the camera with HEGP were respectively 14.6 mm and 3.84 cpm/kBq at 10 cm from the I-131 source, whereas those with MELP were respectively 14.8 mm and 9.82 cpm/kBq. There was a negligible difference in system resolution between HEGP and MELP, and sensitivity with MELP was higher than that with HEGP because of the septal penetration and radioactive scatter of MELP. Tan et al. [18] reported that the image contrast of I-131-Tositumomab with an HE collimator was greater than that with an ME collimator in whole-body imaging. In addition, the sensitivity of an ME collimator was approximately 2.8-fold higher than that of an HE collimator. Our results with planar imaging were similar to Tan's results with whole-body imaging.

In the simulation of the extra-thyroid beds on whole-body imaging, FWHM with MELP was slightly worse than that with HEGP at all table scan speeds. The %CV of MELP was significantly higher than that of HEGP at a table speed of 20 cm/min because there is a lot of noise in I-131 imaging with MELP at this table speed (Table 2). Tan et al. [18] showed the image contrast at a table speed of 20 cm/min was not significantly different from that at a table speed of 100 cm/min; however, image noise increased with the lower counts at 20 cm/min compared with 100 cm/min. Mah et al. [19] reported that there is no significant difference in I-131 half-life and residence time measurements using the same table speed in whole-body

Table 4 %CV of the SPECT imaging with different pixel sizes and I-131 radioactivity

FWHM (mm)								
Radioactivity (MBq)	0.19		0.37		0.74		1.85	
Pixel size (mm)	MELP	HEGP	MELP	HEGP	MELP	HEGP	MELP	HEGP
2.4	16.2**	14.2	16.1**	14.0	15.3**	13.9	15.2**	13.5
4.8	25.7**	20.0	25.1**	20.3	24.9**	20.5	25.2**	20.3

** $P < 0.01$ vs. HEGP

imaging with HEGP and MELP. Therefore, FWHM and image contrast will not be different between HEGP and MELP in spite of different table speeds in whole-body imaging. Image noise, however, will slightly increase when MELP is applied for whole-body imaging at faster table speeds. In SPECT imaging with different pixel sizes and radioactivity, although FWHM of MELP was a little different from that of HEGP (Table 3), %CV of MELP was significantly higher than that of HEGP (Table 4). Basically, the FWHM of SPECT resolution is independent of the low radioactivity level using filtered back projection of reconstruction algorithm. In our study, OSEM-3D yielded slightly higher SPECT resolution and lower %CV when radioactivity in the phantom was gradually increased from 0.19 to 1.85 MBq. In addition, the OSEM-3D with MELP showed a smaller effect than that with HEGP.

In the simulation of the thyroid beds, the radioactivity of the thyroid beds was appropriate because radioactivity was determined by measurement in the thyroid area of patients with DTC administered 1.11 or 3.70 GBq I-131 using the MIRD method. Only 1.85 MBq phantoms could be distinguished from normal thyroid beds using both collimators in whole-body imaging (Fig. 2). However, MELP yielded more star artifacts than HEGP. SPECT images with MELP could not identify the phantom with low radioactivity of 0.19 and 0.37 MBq because MELP also produced a lot of radioactive scatter and star artifacts, and the phantom with low radioactivity was not different from background radioactivity in the SPECT imaging. HEGP identified the phantom with low radioactivity using OSEM-3D with the resolution correction method (Fig. 3). Koral et al. [20] showed the usefulness of OSEM-3D using a whole-body phantom including I-131 and an HE collimator. When there is a low I-131 radioactivity in the thyroid beds, the effect of resolution correction in the OSEM-3D will be small because radioactivity of the thyroid beds cannot be differentiated from background radioactivity.

Because these simulation studies using phantoms were performed without background radioactivity, we also performed clinical studies with background radioactivity. In patients administered 1.11 GBq I-131, lower uptake of I-131 in the thyroid beds could not be detected using whole-body imaging with MELP because the uptake was buried in the noise of background radioactivity (Fig. 4a).

However, the uptake was detected using whole-body imaging with HEGP and SPECT imaging with both collimators (Fig. 4b–d). This is because HEGP has lower septal penetration than MELP, and use of OSEM-3D and a resolution correction method with SPECT imaging reduced the image noise and improved image contrast. In another patient administered 1.11 GBq I-131, there was extensive I-131 uptake in the thyroid beds compared with the other patient, as shown in the Fig. 4. Although we could not detect extra-thyroid beds in the whole-body imaging with MELP because of star artifacts, whole-body imaging with HEGP decreased the amount of star artifacts and was able to detect the extra-thyroid beds (Fig. 5a, c). On the other hand, SPECT images with both collimators could differentiate the thyroid beds (Fig. 5b, d). In the United States, some European countries and Japan, I-131 at ≤1.11 GBq is sufficient for ablation treatment of patients with DTC as outpatients [5, 21–23]. In addition, to maximize cost-effectiveness such as application of MELP, some hospitals that can perform I-131 ablation do not have an HE collimator and inpatient facility. In that case, it will be useful to perform I-131 ablation imaging with ME collimators as an outpatient treatment.

In two patients administered 3.70 GBq I-131, whole-body images with MELP could not identify thyroid beds in one patient with DTC exhibiting low uptake of I-131 in thyroid beds because of the presence of many star artifacts (Fig. 6a), whereas whole-body imaging with HEGP and SPECT imaging with both collimators were able to differentiate the thyroid beds (Fig. 6b–d). OSEM-3D, which decreased image noise and increased image contrast, had a significant effect on the SPECT imaging. In thyroid beds with higher uptake of I-131, there were no differences in whole-body and SPECT imaging between the collimators, although MELP also yielded star artifacts. In this patient, there was extensive thyroid uptake of I-131 compared with background radioactivity and star artifacts. In this case, although SPECT imaging may not be necessary in MELP, the increased uptake may be caused by star artifacts merging with regions of I-131 uptake representing thyroid cancer and/or lymph node metastases. Therefore, when selecting MELP in the whole-body imaging of ablation treatment using 1.11 and 3.70 GBq I-131, SPECT imaging should be added to differentiate clearly thyroid beds,

thyroid cancers and/or lymph node metastases, and OSEM-3D should be applied for reconstruction of the SPECT data.

Conclusion

It is important to locate thyroid beds, extra-thyroid beds and/or lymph node metastases after NaI-131 ablation treatment in order to monitor the efficacy of ablation in patients with DTC. Although HEGP is the best collimator for imaging I-131 ablation, MELP can be applied to not only whole-body imaging but also SPECT imaging if HEGP cannot be used.

Conflict of interest   There are no conflicts of interest.

References

1. Sherman SI. Thyroid carcinoma. Lancet. 2003;361:501–11.
2. Hay ID, McConahey WM, Goellner JR. Managing patients with papillary thyroid carcinoma: insights gained from the Mayo Clinic's experience of treating 2,512 consecutive patients during 1940 through 2000. Trans Am Clin Climatol Assoc. 2002;113:241–60.
3. McGriff NJ, Csako G, Gourgiotis L, Lori CG, Pucino F, Sarlis NJ. Effects of thyroid hormone suppression therapy on adverse clinical outcomes in thyroid cancer. Ann Med. 2002;34:554–64.
4. ICRP. Release of patients after therapy with unsealed radionuclides. Publication 94. Ann ICRP. 2004;34(2).
5. Klerk JMH. ^{131}I therapy: inpatient or outpatient? J Nucl Med. 2000;41:1876–8.
6. Filesi M, Signore A, Ventroni G, Melacrinis FF, Ronga G. Role of initial iodine-131 whole-body scan and serum thyroglobulin in differentiated thyroid carcinoma metastases. J Nucl Med. 1998;39(9):1542–6.
7. Tharp K, Israel O, Hausmann J, Bettman L, Martin WH, Daitzchman M, et al. Impact of ^{131}I-SPECT/CT images obtained with an integrated system in the follow-up of patients with thyroid carcinoma. Eur J Nucl Med Mol Imaging. 2004;31:1435–42.
8. Chen L, Luo Q, Shen Y, Yu Y, Yuan Z, Lu H, et al. Incremental value of ^{131}I SPECT/CT in the management of patients with differentiated thyroid carcinoma. J Nucl Med. 2008;49:1952–7.
9. Fleming JS, Alaamer AS. Influence of collimator characteristics on quantification in SPECT. J Nucl Med. 1996;37:1832–6.
10. Luster M, Clarke SE, Dietlein M, Lassmann M, Lind P, Oyen WJ, et al. Guidelines for radioiodine therapy of differentiated thyroid cancer. Eur J Nucl Med Mol Imaging. 2008;35:1941–59.
11. Specht HD, Brown PH, Hanada JM, Miley AA. Importance of collimator selection for quantitative 131I scintigraphy. Nucl Med Commun. 1991;12:645–54.
12. Hung BT, Huang SH, Huang YE, Wang PW. Appropriate time for post-therapeutic I-131 whole body scan. Clin Nucl Med. 2009;34:339–42.
13. Kobayashi M, Wakabayashi H, Kojima H, Konishi T, Okuda K, Yoneyama H, et al. Prototype imaging protocols for monitoring the efficacy of iodine-131 ablation in differentiated thyroid cancer. Hell J Nucl Med. 2013;16:175–80.
14. Kappadath SC, Erwin WD, Wendt RE. 3rd: observed inter-camera variability of clinically relevant performance characteristics for Siemens Symbia gamma cameras. J Appl Clin Med Phys. 2006;7:74–80.
15. Zeintl J, Vija AH, Yahil A, Hornegger J, Kuwert T. Quantitative accuracy of clinical ^{99m}Tc SPECT/CT using ordered-subset expectation maximization with 3-dimensional resolution recovery, attenuation, and scatter correction. J Nucl Med. 2010;51:921–8.
16. Rasband, WS, Image J. U. S. National Institutes of Health, Bethesda, Maryland, USA, http://imagej.nih.gov/ij/, 1997–2012.
17. Cooper DS, Doherty GM, Haugen BR, Kloos RT, Lee SL, Mandel SJ, et al. Revised American Thyroid Association management guidelines for patients with thyroid nodules and differentiated thyroid cancer. Thyroid. 2009;19:1167–214.
18. Tan HK, Wassenaar RW, Zeng W. Collimator selection, acquisition speed, and visual assessment of 131I-tositumomab biodistribution in a phantom model. J Nucl Med Technol. 2006;34:224–7.
19. Mah E, Spicer KM. Comparison of medium- and high-energy collimators for ^{131}I-tositumomab dosimetry. J Nucl Med Technol. 2007;35:148–53.
20. Koral KF, Yendiki A, Dewaraja YK. Recovery of total I-131 activity within focal volumes using SPECT and 3D OSEM. Phys Med Biol. 2007;52:777–90.
21. Bal CS, Kumar A, Pant GS. Radioiodine dose for remnant ablation in differentiated thyroid carcinoma: a randomized clinical trial in 509 patients. J Clin Endocrinol Metab. 2004;89:1666–73.
22. Schlumberger M, Catargi B, Borget I, Deandreis D, Zerdoud S, Bridji B, et al. Strategies of radioiodine ablation in patients with low-risk thyroid cancer. N Engl J Med. 2012;366:1663–73.
23. Notification on release of patients after administration of radioactive pharmaceuticals No. 70, Pharmaceutical and Food Safety Bureau, Ministry of Health, Labour and Welfare, 30 June 1998.